

# Optoelectronic properties of defective MoS<sub>2</sub> and WS<sub>2</sub> monolayers

Saboura Salehi<sup>1</sup> and Alireza Saffarzadeh<sup>1,2,\*</sup>

<sup>1</sup>*Department of Physics, Payame Noor University, P.O. Box 19395-3697 Tehran, Iran*

<sup>2</sup>*Department of Physics, Simon Fraser University, Burnaby, British Columbia, Canada V5A 1S6*

(Dated: June 7, 2021)

We theoretically explore the effect of metal and disulphur vacancies on electronic and optical properties of MoS<sub>2</sub> and WS<sub>2</sub> monolayers based on a Slater-Koster tight-binding model and including the spin-orbit coupling. We show that the vacancy defects create electronic flat bands by shifting the Fermi level towards the valence band, indicating that both types of vacancies may act as acceptor sites. The optical spectra of the pristine monolayers show step-like features corresponding to the transition from spin split valence band to the conduction band minimum, whereas the defective monolayers exhibit additional peaks in their spectra arising from induced midgap states in their band structures. We find that Mo and W vacancies contribute mostly in the low-energy optical spectrum, while the S<sub>2</sub> vacancies enhance the optical conductivity mainly in the visible range of the spectrum. This suggests that depending on the type of vacancy, the atomic defects in MoS<sub>2</sub> and WS<sub>2</sub> monolayers may increase the efficiency of solar cells used in photovoltaic systems.

PACS numbers:

## I. INTRODUCTION

Two-dimensional (2D) transition metal dichalcogenides (TMDs) have attracted increasing attention because of their unique physical and chemical properties<sup>1,2</sup>. These materials with the general formula MX<sub>2</sub> have a layered structure in the form of X-M-X where M is a transition metal from group IV, V, or VI and X is a chalcogen. Due to their indirect-to-direct bandgap and tunable electronic properties, they can be potentially used for many electronic and optoelectronic applications. For instance, MoS<sub>2</sub> and WS<sub>2</sub> monolayers with band gaps allowing absorption in the visible region of the electromagnetic spectrum can be utilized in field-effect transistors, solar cells, and electroluminescent devices<sup>3-6</sup>.

Due to the presence of spin-orbit coupling in monolayer of MX<sub>2</sub>, their valence band is split at the K-point of the Brillouin zone and therefore, direct transitions between the maxima of the split valence bands and the minimum of the conduction band can occur<sup>3,6-8</sup>. In this regard, recent optical measurements of MoS<sub>2</sub> have shown two main peaks corresponding to A and B exciton bands which are related to such a spin splitting<sup>6,8</sup>. In fact, the experimental absorption spectra have focused mainly on the A and B exciton transitions. Moreover, optical properties of pristine TMD monolayers have also been theoretically studied by several groups using first principles calculations<sup>9-12</sup>, Slater-Koster tight-binding model<sup>13,14</sup> and equation of motion approach<sup>15</sup>.

On the other hand, structural defects, such as vacancies, dislocations, and grain boundaries have been observed in pristine TMD monolayers<sup>16-18</sup>. Application of these defects to improve the optoelectronic properties of the monolayers is highly desirable. Accordingly, atomic defects in TMD materials have been studied both theoretically and experimentally<sup>19-23</sup>.

Vacancy defects in TMD monolayers can be created by thermal annealing and  $\alpha$  particles<sup>24</sup> or electron and ion beam irradiation<sup>17,25,26</sup>. Introduction of these defects in the structures forms localized trap states in the bandgap region which lead to light emission at energies lower than the interband op-

tical transition energy<sup>24,26</sup>. In this context, Khan et al.<sup>23</sup> have recently studied optical susceptibilities of single-layer TMDs in the presence of vacancy defects using first-principles calculations. They showed that the localized defect states induce sharp transitions in optical susceptibility spectrum and a simple tight-binding model can reveal the essential features of the localized defect states in electronic band structures. The localized excitonic states related to vacancy defects can tune the band gap<sup>27</sup> and serve as single-photon emitters<sup>21,22</sup>. Experimental observations have shown that monosulphur vacancies are the most abundant defects. However, their behavior as an acceptor<sup>30</sup> or a donor<sup>1,16,28,29,31,32</sup> is still under debate. Indeed, charge transfer with substrate and also impurities such as rhenium which is present in the environment can play a significant role in the type of doping in TMD monolayers with S vacancies<sup>30</sup>. Nevertheless, the Mo and W point defects can make the system a p-type semiconductor<sup>28,30</sup>.

In this work, based on a parameterized tight-binding model which includes the spin-orbit coupling and ignores the electron-hole interaction, we investigate the influence of metal and disulphur vacancy defects at two different concentrations on electronic and optical properties of MoS<sub>2</sub> and WS<sub>2</sub> monolayers. Although disulphur vacancies in TMD materials may lead to recombination of surface atoms and cause some distortions in the monolayer structures<sup>17</sup>, such effects are ignored in our theory. It is shown that the atomic defects strongly affect the joint density of states (JDOS) and optical properties of the pristine monolayers by inducing mid-gap states in the band structure of these materials. Moreover, the step-like features in the optical spectrum of defect-free structures, induced by spin-orbit coupling may change by introducing the vacancy defects. To do this, in Section 2 we introduce our model and formalism for calculation of electronic band structure, JDOS, and optical conductivity of the pristine and defective monolayers. Numerical results and discussion for both MoS<sub>2</sub> and WS<sub>2</sub> monolayers with different types and concentrations of vacancy defects are presented in Section 3. A brief conclusion is given in Section 4.

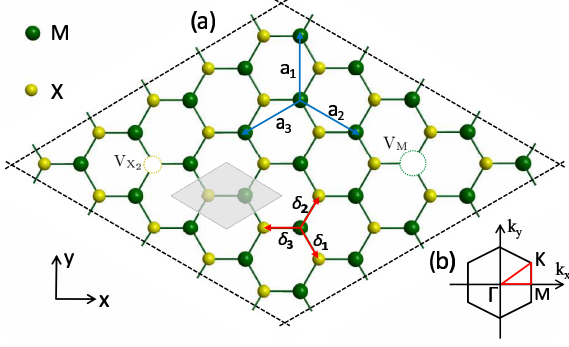


FIG. 1: (Color online) (a) Top view of a  $5 \times 5$  single-layer  $\text{MX}_2$  supercell containing a single M or  $\text{X}_2$  vacancy ( $V_M$  or  $V_{\text{X}_2}$ ). The nearest and the next nearest neighbors are shown by vectors  $\delta_i$  and  $a_i$ , respectively. The grey area shows the unit cell of pristine  $\text{MX}_2$  monolayer. (b) Hexagonal Brillouin zone of a  $\text{MX}_2$  monolayer with the red lines along which the band structures are calculated.

## II. MODEL AND FORMALISM

To study the electronic and optical properties of defective  $\text{MoS}_2$  and  $\text{WS}_2$  monolayers we use a six-band tight-binding approximation which is computationally inexpensive compared to other approaches such as 11-band method<sup>33,34</sup> and non-orthogonal model with  $sp^3d^5$  orbitals<sup>35</sup>. The model is based on the three  $4d$ -orbitals of the transition metal atoms (Mo/W),  $d_{xy}$ ,  $d_{x^2-y^2}$ , and  $d_{3z^2-r^2}$  with dominant contribution in the valence and conduction bands of  $\text{MX}_2$  monolayers around the Fermi energy, and also the symmetric (anti-symmetric) combinations of  $3p$ -orbitals of the top and bottom chalcogen atoms S, i.e.,  $p_x$ ,  $p_y$  ( $p_z$ )<sup>14,33,34,36</sup>. The basis vector for electrons with spin  $\sigma = \uparrow, \downarrow$  can be expressed as

$$|\Phi_\sigma\rangle = (d_{3z^2-r^2,\sigma}, d_{x^2-y^2,\sigma}, d_{xy,\sigma}, p_{x,\sigma}^+, p_{y,\sigma}^+, p_{z,\sigma}^-)^T \quad (1)$$

where  $p_i^\nu = (p_i^t + \nu p_i^b)/\sqrt{2}$  with  $\nu = \pm$ ,  $i = x, y, z$ , and  $t(b)$  refers to the top (bottom) chalcogen atom. In order to model a defective  $\text{MX}_2$  monolayer with different vacancy concentrations the structure is partitioned into  $n \times n$  supercells each containing  $n^2$  unit cells where  $n$  is an integer number. Fig. 1(a) shows a  $5 \times 5$  supercell containing X or M vacancies. An atomic vacancy can be modeled by removing one X or M atom from each supercell without any relaxation of atomic positions. Considering the basis set in Eq. (1), the tight-binding Hamiltonian of the  $\text{MX}_2$  monolayers can be written as

$$H = H_{SK} \otimes \mathbf{1} + H_{SO}, \quad (2)$$

with

$$H_{SK} = \sum_{i,j} \sum_{\alpha,\beta} (\epsilon_{i\alpha} \delta_{ij} \delta_{\alpha\beta} + t_{i\alpha,j\beta}) b_{i\alpha}^\dagger b_{j\beta}, \quad (3)$$

$$H_{SO} = \sum_i \sum_{\sigma,\sigma'} \frac{\lambda_i}{2\hbar} \mathbf{L}_i \cdot \boldsymbol{\tau}_{\sigma\sigma'}, \quad (4)$$

where  $H_{SK}$  and  $H_{SO}$  represent the Slater-Koster tight-binding Hamiltonian<sup>37</sup> and the spin-orbit coupling term, respectively, and  $\mathbf{1}$  is the  $2 \times 2$  identity matrix for spin of electron. Here,  $b_{i\alpha}^\dagger$  ( $b_{i\alpha}$ ) is the creation (annihilation) operator for an electron in the atomic orbital  $\alpha$  at  $i$ -th atom,  $\varphi_{i\alpha}$ , with on-site energy  $\epsilon_{i\alpha}$ . The interatomic hopping parameters,  $t_{i\alpha,j\beta} = \langle \varphi_{i\alpha} | H_{SK} | \varphi_{j\beta} \rangle$ , between atomic orbitals  $\varphi_{i\alpha}$  and  $\varphi_{j\beta}$  depend on the Slater-Koster TB parameters and directional cosines of the vector connecting the corresponding atoms. These parameters are related to hopping processes between nearest neighbors M-M, X-X, and M-X. See vectors  $\mathbf{a}_i$  and  $\delta_i$  ( $i=1, 2$ , and  $3$ ) in Fig. 1(a). The hopping terms between next nearest neighbors are ignored in this model. In Eq. 4,  $\boldsymbol{\tau}$  are the Pauli spin matrices,  $\mathbf{L}_i$  is the atomic angular momentum operator, and  $\lambda_i$  is the intra-atomic spin-orbit coupling constant which depends on the type of atom  $i$ . The spin-orbit coupling leads to a strong spin-splitting in the valence-band maximum (VBM), especially in  $\text{WS}_2$  monolayers<sup>38</sup>. Therefore, the inclusion of this interaction which is necessary for obtaining the correct band structures can affect optical spectrum of the TMD monolayers by inducing new optical transitions.

The spin-dependent Hamiltonian in  $\mathbf{k}$ -space for a pristine  $\text{MX}_2$  monolayer is given by  $H = \sum_{\mathbf{k},\sigma} H(\mathbf{k}, \sigma)$  with

$$H(\mathbf{k}, \sigma) = \begin{pmatrix} H_{MM}(\mathbf{k}, \sigma) & H_{MX}(\mathbf{k}) \\ H_{MX}^\dagger(\mathbf{k}) & H_{XX}(\mathbf{k}, \sigma) \end{pmatrix}, \quad (5)$$

$$H_{MM(XX)}(\mathbf{k}, \sigma) = E_{M(X)}(\sigma) + 2 \sum_{i=1}^3 T_i^{\text{MM}(XX)} \cos(\mathbf{k} \cdot \mathbf{a}_i), \quad (6)$$

$$H_{MX}(\mathbf{k}) = \sum_{i=1}^3 T_i^{\text{MX}} \exp(-i\mathbf{k} \cdot \delta_i), \quad (7)$$

where  $E_{M(X)}$ ,  $T_i^{\text{MM}(XX)}$ , and  $T_i^{\text{MX}}$  are  $3 \times 3$   $\mathbf{k}$ -independent matrices. These matrices depend on the Slater-Koster parameters only and are given in Ref. [14]. Note that although the band structures of pristine  $\text{MoS}_2$  and  $\text{WS}_2$  presented in Ref. [14] are correct, the given Slater-Koster parameters therein cannot reproduce the correct band structure of  $\text{WS}_2$ . Therefore, the parameters for  $\text{MoS}_2$  and  $\text{WS}_2$  monolayers with a minor correction are given in Table. I.

To investigate the optical response of a defective TMD monolayer to a linearly polarized light we study joint density of states (JDOS) and real part of optical conductivity. The JDOS provides a measure of the number of allowed optical transitions between the occupied electronic states of the valence band and the unoccupied electronic states of the conduction band separated by energy  $\hbar\omega$ :

$$\text{JDOS}(\omega) = \sum_{mn\sigma} \sum_{\mathbf{k}} \delta(\epsilon_{mn}^\sigma(\mathbf{k}) - \hbar\omega), \quad (8)$$

where  $\omega$  is the light frequency and  $\epsilon_{mn}^\sigma(\mathbf{k}) = \epsilon_m^\sigma(\mathbf{k}) - \epsilon_n^\sigma(\mathbf{k})$  is the transition energy between occupied band  $n$  and empty

band  $m$ . Therefore, the JDOS represents the number of states that can undergo energy and  $\mathbf{k}$ -conserving (direct) transitions for photon frequencies between  $\omega$  and  $\omega + d\omega$ .

Moreover, in the electric-dipole approximation, the momentum matrix element for an interband electronic transition from the eigenstate  $|n, \mathbf{k}, \sigma\rangle$  in an occupied band to the eigenstate  $|m, \mathbf{k}, \sigma\rangle$  in an empty band is given by  $p_{x,mn}^\sigma = \langle m, \mathbf{k}, \sigma | \hat{p}_x | n, \mathbf{k}, \sigma \rangle$  which is assumed that the electromagnetic field is along the  $x$ -direction. The momentum operator is given by  $\hat{\mathbf{p}} = (m/\hbar)\nabla H(\mathbf{k}, \sigma)$ . Note that the matrix elements  $p_{x,mn}^\sigma$  determine whether the transition is allowed or forbidden. A zero momentum-matrix element means a forbidden transition. However, the transition is allowed when the symmetry of  $p_{x,mn}^\sigma$  spans the totally symmetric representation of the point group to which the unit cell belongs. Therefore, the real part of optical conductivity can be obtained from the Kubo formula<sup>39</sup>; i.e.,

$$\sigma_{xx}(\omega) = \frac{e^2}{4\pi m^2 \omega} \sum_{mn\sigma} \int_{1\text{BZ}} |p_{x,mn}^\sigma|^2 \delta(\varepsilon_{mn}^\sigma(\mathbf{k}) - \hbar\omega) d^2\mathbf{k}, \quad (9)$$

where  $e$  is the electron charge and  $m$  is the electron mass. The two-dimensional integral is carried over the first Brillouin zone.

Note that the Dirac delta function in Eqs. (8) and (9) is approximated by a Lorentzian function with a broadening factor of 0.005 eV. In addition, we use a  $500 \times 500$   $\mathbf{k}$ -point mesh for accurate Brillouin zone integrations.

TABLE I: The spin-orbit coupling (SOC) and Slater-Koster tight-binding parameters of MoS<sub>2</sub> and WS<sub>2</sub> monolayers (taken from Ref. [14] with a minor correction in  $V_{pd\sigma}$  of W-S). All values are in units of eV.

		MoS <sub>2</sub>	WS <sub>2</sub>
SOC	$\lambda_M$	0.086	0.271
	$\lambda_X$	0.052	0.057
	$\Delta_0$	-1.094	-1.155
Crystal Fields	$\Delta_1$	-0.050	-0.650
	$\Delta_2$	-1.511	-2.279
	$\Delta_p$	-3.559	-3.864
	$\Delta_z$	-6.886	-7.327
M-S	$V_{pd\sigma}$	3.689	4.911
	$V_{pd\pi}$	-1.241	-1.220
M-M	$V_{dd\sigma}$	-0.895	-1.328
	$V_{dd\pi}$	0.252	0.121
	$V_{dd\delta}$	0.228	0.442
S-S	$V_{pp\sigma}$	1.225	1.178
	$V_{pp\pi}$	-0.467	-0.273

### III. RESULTS AND DISCUSSION

To study the influence of atomic vacancy defects on the electronic and the optical properties of MoS<sub>2</sub> and WS<sub>2</sub> monolayers we first discuss the band structure, JDOS, and optical conductivity of the pristine monolayers. Figs. 2(a) and (b) show the band structures with the projection of spin operator

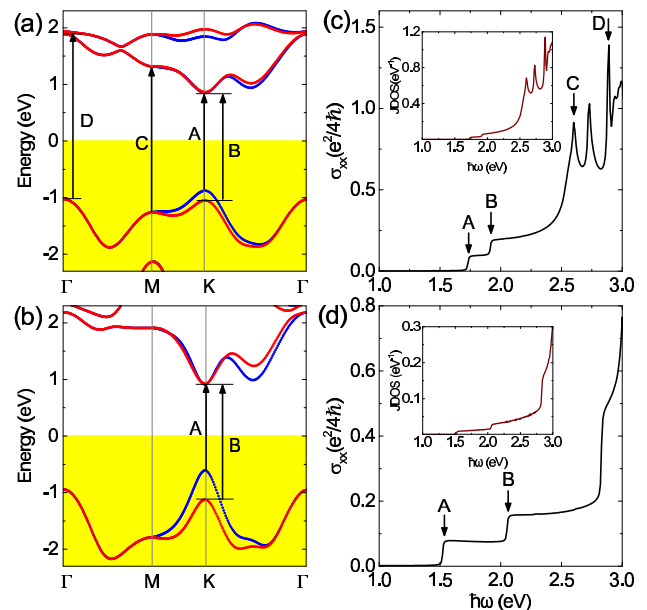


FIG. 2: (Color online) (a)((b)) Calculated band structure with projection of spin operator and (c)((d)) the real part of optical conductivity of pristine MoS<sub>2</sub> (WS<sub>2</sub>) monolayer. The red and blue colors in the band structures indicate the spin-up and spin-down states, respectively. The insets show the corresponding JDOS. The intersection of white and yellow regions in (a) and (b) shows the Fermi energy. The arrows A, B, C, and D denote some important interband optical transitions.

in the energy range of  $|E| \leq 2.3$  eV for MoS<sub>2</sub> and WS<sub>2</sub> monolayers, respectively. The splitting of the valence band at the K point in WS<sub>2</sub> is more than two times larger than that in MoS<sub>2</sub>, which makes WS<sub>2</sub> monolayers a potential candidate for spin- and valley-based electronic devices<sup>40</sup>. Note that the order of spin bands in the band structures along  $\Gamma$ -K'-M (not shown here) will flip compared to those along the  $\Gamma$ -K-M lines<sup>32</sup>. This feature leads to a valley-selective optical absorption using a circularly polarized light which may cause optically induced valley and spin Hall effects<sup>41</sup>. The difference in the valence band spin-splitting between MoS<sub>2</sub> and WS<sub>2</sub> monolayers is directly reflected in their JDOS and optical spectra, as shown in Figs. 2(c) and 2(d). The interband transitions from the valence bands to the conduction bands can produce plateaus (shoulders) at lower energies and a series of sharp peaks at higher energies in the optical spectra which are attributed to the van Hove singularities in the JDOS, shown in the insets of Fig. 2. The arrows, marked by A, B, C, and D in the band structures of the two compounds, are related to some of these transitions. Comparison of the van Hove singularities in the JDOS with the plateaus and sharp peaks in the optical conductivity reveals that the related optical transitions of the pristine monolayers in the given energy range are all allowed. The interband transitions A and B correspond to the direct excitonic transitions which have been observed in the photoluminescence measurements<sup>3,42</sup>. Note that in order to qualitatively treat the excitonic effects in 2D materials such as monolayers MoS<sub>2</sub> and WS<sub>2</sub>, the effective Coulomb inter-

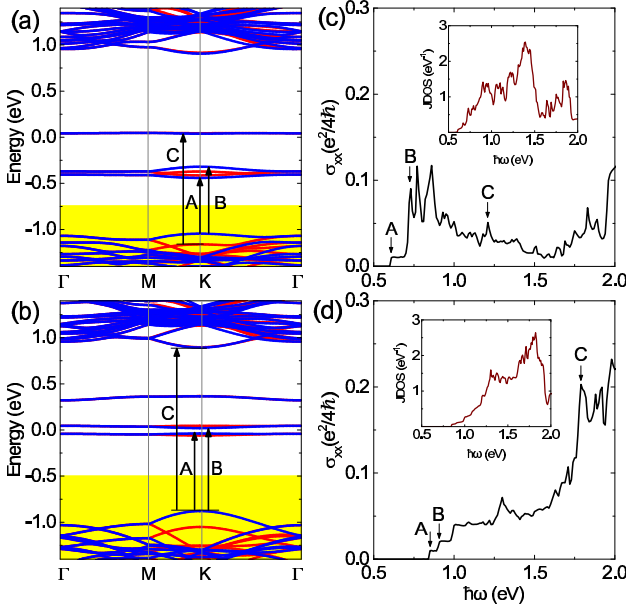


FIG. 3: Calculated band structures, optical conductivities, and joint densities of states (insets) of MoS<sub>2</sub> monolayer with  $5 \times 5$  supercells for (a,c)  $V_{\text{Mo}}$  and (b,d)  $V_{\text{S}_2}$ . The arrows A, B, and C denote some important interband optical transitions. The intersection of white and yellow regions in (a) and (b) shows the Fermi energy.

action between electrons and holes should be included in the theory<sup>13</sup>.

It is worth mentioning that although the momentum matrix elements  $p_{x,mn}^\sigma$  and  $p_{y,mn}^\sigma$  have different  $\mathbf{k}$ -dependencies, the  $\mathbf{k}$  integral over the whole Brillouin zone in the Kubo formula<sup>39</sup> gives the same optical conductivities  $\sigma_{xx}(\omega)$  and  $\sigma_{yy}(\omega)$ , indicating that the optical spectra of pristine MX<sub>2</sub> monolayers are isotropic. Such a feature has also been reported for graphene at low and high frequencies<sup>43</sup>.

Now, we investigate the influence of Mo, W, and S<sub>2</sub> vacancies on the optical properties of the layered structures. To control the vacancy concentration, we use the supercell approach in which a perfect monolayer is described as an infinite periodic array of  $n \times n$  supercells<sup>32</sup>. Then a vacancy defect is created by removing one atom from each supercell without any change in the symmetry of the lattice (see Fig. 1(a)). Note that in the supercell approach the corresponding Brillouin zone shrinks in size and the bands get folded. We refer to a single Mo(W) vacancy as  $V_{\text{Mo(W)}}$ , whereas vacancies of two sulphur atoms (one at the top layer and the other at the bottom layer of MX<sub>2</sub>) attached to the same Mo/W atom are denoted as  $V_{\text{S}_2}$  (see Fig. 1).

Figs. 3(a) and (b) show the band structures of MoS<sub>2</sub> in  $5 \times 5$  supercells with  $V_{\text{Mo}}$  and  $V_{\text{S}_2}$ , respectively. For this case, the concentration of  $V_{\text{Mo}}$  is  $\frac{1}{75}$ , while it is  $\frac{2}{75}$  for  $V_{\text{S}_2}$ , corresponding to defect densities  $\sim 4.6 \times 10^{13} \text{ cm}^{-2}$  and  $9.2 \times 10^{13} \text{ cm}^{-2}$ , respectively. The vacancy states which are mainly localized around atomic defects<sup>19</sup> induce several narrow (flat) bands for each spin subband around zero energy in the band structures<sup>44</sup>. Although the midgap states are almost degener-

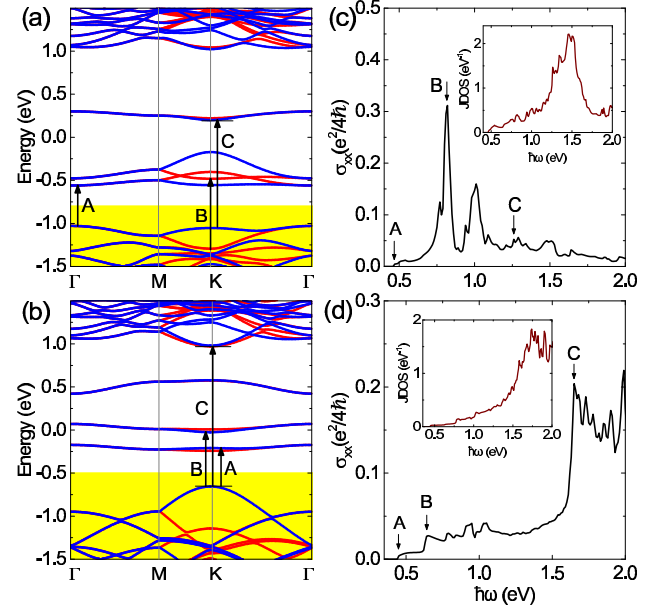


FIG. 4: Calculated band structures, optical conductivities, and joint densities of states (insets) of WS<sub>2</sub> monolayer with  $5 \times 5$  supercells for (a,c)  $V_{\text{W}}$  and (b,d)  $V_{\text{S}_2}$ . The arrows A, B, and C denote some important interband optical transitions. The intersection of white and yellow regions in (a) and (b) shows the Fermi energy.

ate, the spin splitting in the valence bands makes some of the interband transitions spin dependent (e.g., see transition C in Fig. 3(a)). The tendency of defect states in Fig. 3(a) towards the valence band predicts the *p*-type semiconducting behavior by introducing Mo vacancies in this structure. For the case of  $V_{\text{S}_2}$ , however, there is a tendency towards the primary conduction band (see Fig. 3(b)). We should mention that the position of Fermi energy, shown in the figures, is determined by counting the number of electrons that the atoms in the supercell provide. These electrons fill up the lowest spin dependent energy bands and hence, the Fermi level lies between the highest occupied band and the lowest unoccupied band. In other words, since the energy bands are spin dependent, all the bands below the Fermi energy are singly occupied.

Optical conductivity and JDOS of MoS<sub>2</sub> monolayer with  $V_{\text{Mo}}$  and  $V_{\text{S}_2}$  are depicted in Figs. 3(c) and (d), respectively. Some interband transitions in the band structures, marked by A, B, and C are shown in the optical spectra. The optical transitions for the structure with  $V_{\text{Mo}}$  can occur at photon energies  $\hbar\omega \geq 0.6\text{eV}$ , whereas, these transitions for the monolayer with  $V_{\text{S}_2}$  start at  $\hbar\omega = 0.84\text{eV}$ . Due to more flat bands in the band gap, the sulphur vacancies induce more plateaus compared to  $V_{\text{Mo}}$ . Moreover, the joint densities of states show different features compared to the optical spectra, indicating that there are considerable forbidden transitions in the defective MoS<sub>2</sub> spectrum as discussed above.

The band structures of WS<sub>2</sub> monolayers with  $V_{\text{W}}$  and  $V_{\text{S}_2}$  are shown in Figs. 4(a) and (b). We see that the difference between the valence band maximum and the lowest defect state in energy is almost the same for both vacancies. Although there is a tendency towards valence band for the  $V_{\text{W}}$ -related



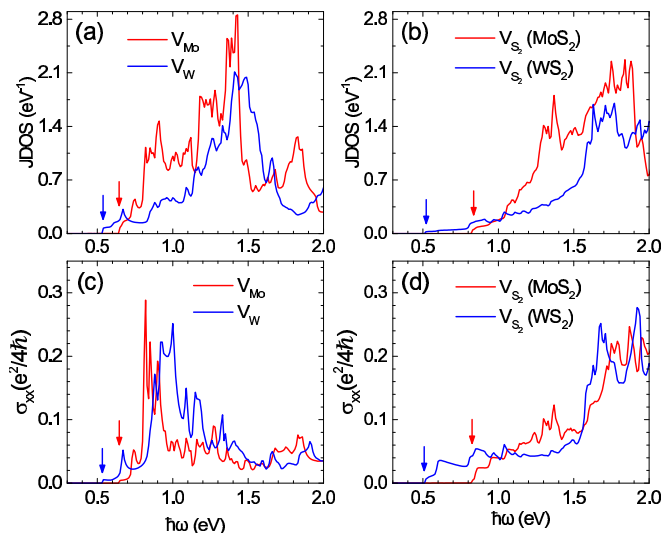


FIG. 5: (a,b) Joint densities of states and (c,d) optical conductivities of defective monolayers MoS<sub>2</sub> (red lines) and WS<sub>2</sub> (blue lines) with 4×4 supercells. The arrows indicate the energies at which the optical transitions begin.

midgap states, such a tendency is weaker for the  $V_{\text{Mo}}$ -related states in MoS<sub>2</sub> monolayer. On the contrary, the energy difference between the conduction band minimum and the highest  $V_{\text{S}_2}$ -related state is almost the same as that between the valence band maximum and the lowest midgap state. Optical conductivity and the joint densities of states are shown in Figs. 4(c) and (d). As can be seen, the energy of first interband transition (marked A) is almost the same for  $V_{\text{W}}$  and  $V_{\text{S}_2}$  in WS<sub>2</sub> structure. Due to the  $V_{\text{S}_2}$ -related flat bands in the band gap, the optical conductivity spectrum exhibits mainly a step-like behavior for photon energies  $\hbar\omega \leq 1.2$  eV, compared to that for the monolayer with  $V_{\text{W}}$ . This feature can also be seen in the JDOS of the structure containing  $V_{\text{S}_2}$ . Again, there are some forbidden optical transitions in the defective structures with whether W or S<sub>2</sub> vacancies, due to the remarkable differences between joint densities of states and the optical spectra.

The optical conductivity can sharply reach a high value at low-energy spectrum when W vacancies are introduced. In this case, an optical transition, marked B in Figs. 4(a) and (c), from valence band to midgap states occurs. However, in the case of S<sub>2</sub> vacancies the conductivity increases sharply when a transition from valence band to conduction band happens (see the transition C in Fig. 4(b) and (d)). Qualitatively, similar features can also be seen in the optical spectra of the defective MoS<sub>2</sub> structure (see Fig. 3). This suggests that the metal vacancies contribute mainly in the low-energy optical spectrum, while the disulphur vacancies contribute mainly in the transitions with higher energies. Therefore, depending on the type of vacancy, the atomic defects in MoS<sub>2</sub> and WS<sub>2</sub> monolayers as sunlight absorbers may increase the efficiency of solar cells used in photovoltaic systems<sup>45</sup>.

We have also performed the tight-binding calculations on a smaller supercell, i.e., 4 × 4, which corresponds to the higher vacancy densities  $\sim 7.2 \times 10^{13} \text{ cm}^{-2}$  ( $V_{\text{Mo/W}}$ ) and

$14.4 \times 10^{13} \text{ cm}^{-2}$  ( $V_{\text{S}_2}$ ). The joint densities and optical conductivity spectra for the monolayers with Mo, W, and S<sub>2</sub> vacancies are depicted in Fig. 5. At higher defect densities the hybridization of vacancy electronic states increases due to the reduction of spatial separation between the vacant sites. As a result, the energy of midgap states are shifted compared to that at low defect concentration. To see this feature one can compare the energies at which the first optical transition (or the first van Hove singularity in the joint densities of states) occur in the defective structures with 5 × 5 and 4 × 4 supercells. In the structures with 4 × 4 supercells, the energies of first optical transitions, marked by red and blue arrows in Fig. 5, increase by 43 meV and 61 meV for Mo and W vacancies, respectively, compared to those in Figs. 3 and 4. On the other hand, the first transition for WS<sub>2</sub> structure with S<sub>2</sub> vacancies is 65 meV higher than that in Fig. 4, while it occurs 15 meV lower than that in Fig. 3. Therefore, with increasing the density of metal vacancy in both structures or the density of S<sub>2</sub> vacancy in WS<sub>2</sub> structure, the defect states shift towards the conduction band, indicating that the tendency of *p*-type semiconducting for these types of vacancies decreases with increasing the defect concentration. The position and the strength of optical peaks in Figs. 5(c) and (d) confirm our above discussion that the metal vacancies considerably increase the optical conductivity when the energy of photons is less than the bandgap of the host structures, while the S<sub>2</sub> vacancies enhance the optical conductivity mainly in the visible range of the electromagnetic spectrum. Since the vacancy defects are unavoidable during the synthesis of MX<sub>2</sub> monolayers, these results are of great practical importance.

It is worth mentioning that the metal and disulphur vacancies do not induce any magnetic moments in MoS<sub>2</sub> and WS<sub>2</sub> monolayers<sup>28,46</sup>. By applying a tensile strain<sup>46</sup> or substitutional doping<sup>28</sup>, however, one can change the magnetic properties of these defective structures. Moreover, although the localized midgap states can act as scattering centers and strongly affect electron transport through the material<sup>47</sup>, these defect states are responsible for an increase in photoluminescence intensity<sup>24</sup>. In other words, the defective structures can emit stronger light and are promising for optoelectronic device applications such as light emitting diodes.

#### IV. CONCLUSION

Based on Slater-Koster six-band tight-binding model and including the spin-orbit coupling, we have studied the effect of Mo, W, and disulphur vacancies on electronic and optical properties of MoS<sub>2</sub> and WS<sub>2</sub> monolayers. It is shown that the defect states induce flat bands in the bandgap and shift the Fermi level towards the valence band, suggesting that these vacancies may act as acceptor sites. Moreover, the localized midgap states have the potential to activate new optical transitions with energies less than the bandgap of pristine structures. We found that although the electronic behavior of MoS<sub>2</sub> and WS<sub>2</sub> monolayers in the presence of both types of metal and disulphur vacancies are almost the same, contributions of the metal and disulphur vacancies in the optical conductiv-

ity occur in different ranges of incident photon energy. The disulphur defects activate the optical spectrum in the visible range, while the Mo and W vacancies activate the conductivity mostly at low energies.

Therefore, our findings are able to reveal some electronic and optical features of the defective MoS<sub>2</sub> and WS<sub>2</sub> monolayers using a six-band tight-binding model which is less computationally demanding than the traditional *ab initio* methods.

## Acknowledgement

This work is partially supported by Iran Science Elites Federation (11/66332).

- 
- \* Electronic address: asaffarz@sfu.ca
- <sup>1</sup> B. Radisavljevic, A. Radenovic, J. Brivio, V. Giacometti, and A. Kis, *Nat. Nanotechnol.* **6**, 147 (2011).
  - <sup>2</sup> D. Braga, I.G. Lezama, H. Berger, and A. Morpurgo, *Nano Lett.* **12**, 5218 (2012).
  - <sup>3</sup> Q. H. Wang, K. Kalantar-Zadeh, A. Kis, J. N. Coleman, and M. S. Strano, *Nat. Nanotech.* **7**, 699 (2012).
  - <sup>4</sup> C. Ataca, H. Sahin, and S. Ciraci, *J. Phys. Chem. C* **116**, 8983 (2012).
  - <sup>5</sup> M.L. Tsai, S.H. Su, J.K. Chang, D.S. Tsai, C.H. Chen, C.I. Wu, L.J. Li, L.J. Chen, J.H. He, *ACS Nano* **8** 8317 (2014).
  - <sup>6</sup> A. Splendiani, L. Sun, Y. Zhang, T. Li, J. Kim, C.-Y. Chim, G. Galli, and F. Wang, *Nano Lett.* **10**, 1271 (2010).
  - <sup>7</sup> K.P. Dhakal, D.L. Duong, J. Lee, Honggi Nam, K. Minsu, M. Kan, Y.H. Lee, and J. Kim, *Nanoscale*, **6**, 13028 (2014).
  - <sup>8</sup> K.F. Mak, C. Lee, J. Hone, J. Shan, T.F. Heinz, *Phys. Rev. Lett.* **105**, 136805 (2010).
  - <sup>9</sup> D.Y. Qiu, F.H. Jornada, and S.G. Louie, *Phys. Rev. Lett.* **111**, 216805 (2013).
  - <sup>10</sup> T.C. Berkelbach, M. S. Hybertsen, and D. R. Phys. Rev. B **88**, 045318 (2013).
  - <sup>11</sup> M. Gibertini, F.M.D. Pellegrino, N. Marzari, Marco Polini, *Phys. Rev. B* **90**, 245411 (2014).
  - <sup>12</sup> I.B. Amara, E.B. Salem, and S. Jaziri, *J. Appl. Phys.* **120**, 051707 (2016).
  - <sup>13</sup> M.L. Trolle, G. Seifert and T.G. Pedersen. *Phys. Rev. B* **89**, 235410 (2014).
  - <sup>14</sup> J.Á. Silva-Guillén, P. San-Jose, and R. Roldán, *Appl. Sci.* **6**, 284 (2016).
  - <sup>15</sup> A.J. Chaves, R.M. Ribeiro, T. Frederico, and N.M.R. Peres, *2D Mater.* **4**, 025086 (2017).
  - <sup>16</sup> H. Qiu, T. Xu, Z. Wang, W. Ren, H. Nan, Z. Ni, Q. Chen, S. Yuan, F. Miao, F. Song, G. Long, Y. Shi, L. Sun, J. Wang and X. Wang, *Nat. Comm.* **4**, 2642 (2013).
  - <sup>17</sup> W. Zhou, X. Zou, S. Najmaei, Z. Liu, Y. Shi, J. Kong, J. Lou, P.M. Ajayan, B.I. Yakobson, and J.-C. Idrobo, *Nano Lett.* **13**, 2615 (2013).
  - <sup>18</sup> A.M. Van der Zande, P.Y. Huang, D.A. Chenet, T.C. Berkelbach, Y.M. You, G.H. Lee, T.F. Heinz, D.R. Reichman, D.A. Muller, J.C. Hone, *Nat. Mater.* **12**, 554 (2013).
  - <sup>19</sup> S. Yuan, R. Roldán, M.I. Katsnelson, and F. Guinea, *Phys. Rev. B* **90**, 041402(R) (2014).
  - <sup>20</sup> J. Kunstmann, T.B. Wendumu, and G. Seifert, *Phys. Status Solidi B* **254**, 1600645 (2017).
  - <sup>21</sup> A. Srivastava, M. Sidler, A.V. Allain, D.S. Lembke, A. Kis, and A. Imamoglu, *Nat. Nanotech.* **10**, 491 (2015).
  - <sup>22</sup> Y.-M. He, G. Clark, J.R. Schaibley, Y. He, M.-C. Chen, Y.-J. Wei, X. Ding, Q. Zhang, W. Yao, X. Xu, C.-Y. Lu, and J.-W. Pan, *Nat. Nanotech.* **10**, 497 (2015).
  - <sup>23</sup> M.A. Khan, M. Erementchouk, J. Hendrickson, and M.N. Leuenberger, *Phys. Rev. B* **95**, 245435 (2017).
  - <sup>24</sup> S. Tongay, J. Suh, C. Ataca, W. Fan, A. Luce, J.S. Kang, J. Liu, C. Ko, R. Raghunathanan, J. Zhou, F. Ogletree, J. Li, J.C. Grossman and J. Wu, *Sci. Rep.* **3**, 2657 (2013).
  - <sup>25</sup> Q. Ma, P.M. Odenthal, J. Mann, D. Le, C.S. Wang, Y. Zhu, T. Chen, D. Sun, K. Yamaguchi, T. Tran, M. Wurch, J.L. McKinley, J. Wyrick, K.M. Magnone, T.F. Heinz, T.S. Rahman, R. Kawakami, and L. Bartels, *J. Phys.: Condens. Matter* **25**, 252201 (2013).
  - <sup>26</sup> L. Ma, Y. Tan, M. Ghorbani-Asl, R. Boettger, S. Kretschmer, S. Zhou, Z. Huang, A.V. Krasheninnikov, and F. Chen, *Nanoscale* **9**, 11027 (2017).
  - <sup>27</sup> Y. Huang, J. Wu, X. Xu, Y. Ho, G. Ni, Q. Zou, G. Koon, W. Zhao, A. Castro Neto, G. Eda, C. Shen, and B. Ozyilmaz, *Nano Res.* **6**, 200 (2013).
  - <sup>28</sup> S.-C. Lu and J.-P. Leburton, *Nano. Res. Lett.* **9**, 676 (2014).
  - <sup>29</sup> J. Suh, T.-E. Park, D.-Y. Lin, D. Fu, J. Park, H.J. Jung, Y. Chen, C. Ko, C. Jang, Y. Sun, R. Sinclair, J. Chang, S. Tongay, and J. Wu, *Nano. Lett.* **14**, 6976 (2014).
  - <sup>30</sup> H.-P. Komsa and A.V. Krasheninnikov, *Phys. Rev. B* **91**, 125304 (2015).
  - <sup>31</sup> D. Liu, Y. Guo, L. Fang, and J. Robertson, *Appl. Phys. Lett.* **103**, 183113 (2013).
  - <sup>32</sup> S. Salehi and A. Saffarzadeh, *Sur. Sci.* **651**, 215 (2016).
  - <sup>33</sup> E. Cappelluti, R. Roldán, J. A. Silva-Guillén, P. Ordejón and F. Guinea, *Phys. Rev. B* **88**, 075409 (2013).
  - <sup>34</sup> R. Roldán, M. P. López-Sancho, F. Guinea, E Cappelluti, J. A. Silva-Guillén, and P. Ordejón, *2D Materials* **1**, 034003 (2014).
  - <sup>35</sup> F. Zahid, L. Liu, Y. Zhu, J. Wang, and H. Guo, *AIP Adv.* **3**, 052111 (2013).
  - <sup>36</sup> A. Castellanos-Gomez, R. Roldán, E. Cappelluti, M. Buscema, F. Guinea, H.S.J. van der Zant, and G.A. Steele, *Nano Lett.* **13**, 5361 (2013).
  - <sup>37</sup> J.C. Slater and G. F. Koster, *Phys. Rev.* **94**, 1498 (1954).
  - <sup>38</sup> Z. Cao, M. Harb, S. Lardhi, and L. Cavallo, *J. Phys. Chem. Lett.* **8**, 1664 (2017).
  - <sup>39</sup> P. T. Yu and M. Cardona, *Fundamentals of Semiconductors: Physics and Materials Properties* (Springer, Berlin, 2001).
  - <sup>40</sup> D. Xiao, G-B Liu, W. Feng, X. Xu, and W. Yao, *Phys. Rev. Lett.* **108**, 196802 (2012).
  - <sup>41</sup> E.J. Sie, J.W. McIver, Y.-H. Lee, L. Fu, J. Kong, and N. Gedik, *Nat. Mater.* **14**, 290 (2015).
  - <sup>42</sup> K.F. Mak, K. He, J. Shan, and T.F. Heinz, *Nat. Nanotech.* **7**, 494 (2012).
  - <sup>43</sup> H.-V. Nguyen and V. H. Nguyen, *Phys. Rev. B* **94**, 117401 (2016).
  - <sup>44</sup> Note that by taking a larger supercell such as  $12 \times 12$ , the vacancy density  $\sim 10^{12} \text{ cm}^{-2}$  will be more in line with experimental values. In such a density, the distance between two vacancies becomes considerably large and the interaction between defects will be negligible. Therefore, one can expect that the midgap states become completely dispersionless due to the strong localization of defect states<sup>32</sup>.

- <sup>45</sup> M. Bernardi, M. Palumbo, and J.C. Grossman, *Nano Lett.* **13**, 3664 (2013).
- <sup>46</sup> P. Tao, H. Guo, T. Yanga, and Z. Zhang, *J. Appl. Phys.* **115**, 054305 (2014).
- <sup>47</sup> M. Ghorbani-Asl, A.N. Enyashin, A. Kuc, G. Seifert, and T. Heine *Phys. Rev. B* **88**, 245440 (2013).